AN EFFICIENT IMPLEMENTATION OF THE FINITE-VOLUME METHOD FOR THE SOLUTION OF RADIATION TRANSPORT IN CIRCUIT BREAKERS

A. Mazaheri[a,*], J.Y. Trépanier[a], R. Camarero[a], P. Robin-Jouan[b]

[a] *École Polytechnique de Montréal, 2900 boul. Édouard-Montpetit, Campus de l'Université de Montréal, 2500 chemin de Polytechnique, Montréal (Québec), H3T 1J4, Canada*

[b] *GE Grid-Solutions, Villeurbanne, France*

* ali.mazaheri@polymtl.ca

Abstract. In this paper, we propose to revisit the method to solve the radiation transport equation in circuit breakers to reduce the computation time. It is based on an explicit approach using a space marching algorithm. The method can further be accelerated using a Cartesian grid and using the axisymmetric assumption. Comparisons performed in terms of accuracy and efficiency between the P1 model, the implicit finite-volume discrete ordinate method and the space-marching finite-volume discrete ordinate method show that the explicit approach is more that an order of magnitude faster than the implicit approach, for the same accuracy.

Keywords: Radiation, Circuit-breaker, Finite-volume method, Space-Marching.

1. Introduction

The numerical modeling and simulation of arc-flow interaction in circuit-breakers are based on the solution of compressible fluid flow, coupled with electrical and magnetic field equations. In circuit breakers, during the high current arcing phase, the high plasma temperature (around 20 kK) results in dominant energy transport by radiation, and intense radiation fluxes reach the nozzle material, causing critical vaporization of the nozzle. Consequently, most recent models require accurate solution of the radiative energy transfer. The numerical modeling of the radiation phenomena is highly complex [1, 2] as the radiation field depends on temperature, gas composition, frequency and direction. Over the years, various radiation models have been proposed, often to provide a compromise between accuracy and computation time. The P1 model [3] has been extensively used because of its relatively low computational cost. However, boundary conditions are difficult to apply for this model and the model fails for transparent media [4]. The most recent modeling involve the solution of the radiative transport equation for a small number of frequency bands using finite-volume discretization (FVM) of the angular directions of propagation [5]. Although it is generally admitted that the FVM method is superior in terms of accuracy over the P1 model, its computational cost often limit its usage for practical applications. In the present paper, we revisit the FVM approach and propose, under few assumptions, an explicit low cost extension of the FVM for circuit-breaker arcing simulation.

2. Governing Equations

The radiative transfer equation (RTE) for a non-scattering medium(eg. circuit breaker) in cylindrical

coordinate system is shown in Eq 1:

$$
\begin{aligned}
&\frac{1}{r}\frac{\partial}{\partial r}[\mu r I(\vec{R},\vec{S})] + \frac{1}{r}\frac{\partial}{\partial \varphi_0}[\eta I(\vec{R},\vec{S})] \\
&+ \frac{\partial}{\partial z}[\xi I(\vec{R},\vec{S})] - \frac{1}{r}\frac{\partial}{\partial \phi}[\eta I(\vec{R},\vec{S})] \\
&= -\beta(\vec{R})I(\vec{R},\vec{S}) + \kappa_a(\vec{R})I_b(\vec{R})
\end{aligned}
\tag{1}
$$

In this equation, $\vec{S} = \vec{e}_r \sin\theta \cos\phi + \vec{e}_{\varphi_0}\sin\theta\sin\phi + \vec{e}_z\cos\theta$, $\mu = \sin\theta\cos\phi$, $\eta = \sin\theta\sin\phi$, and $\xi = \cos\theta$ are the cosines of the path $\vec{S}$, κ_a is the absorption coefficient. This equation governs the variation in the radiant intensity $I(\vec{R},\vec{S})$ at a specific location $\vec{R}$ through the length ds in the direction of $\vec{S}$ as shown in Fig. 1.

For an axisymmetric configuration the term of $\dfrac{\partial}{\partial\varphi_0}$ in Eq. 1 is removed and reduces to:

$$
\begin{aligned}
&\frac{1}{r}\frac{\partial}{\partial r}[\mu r I(\vec{R},\vec{S})] + \frac{\partial}{\partial z}[\xi I(\vec{R},\vec{S})] - \frac{1}{r}\frac{\partial}{\partial\phi}[\eta I(\vec{R},\vec{S})] \\
&= -\kappa_a(\vec{R})I(\vec{R},\vec{S}) + \kappa_a I_b(\vec{R})
\end{aligned}
\tag{2}
$$

Assuming a non-scattering medium, the final form of the RTE becomes:

$$
\frac{dI(\vec{R},\vec{S})}{ds} = -\kappa_a I(\vec{R},\vec{S}) + \kappa_a I_b(\vec{R})
\tag{3}
$$

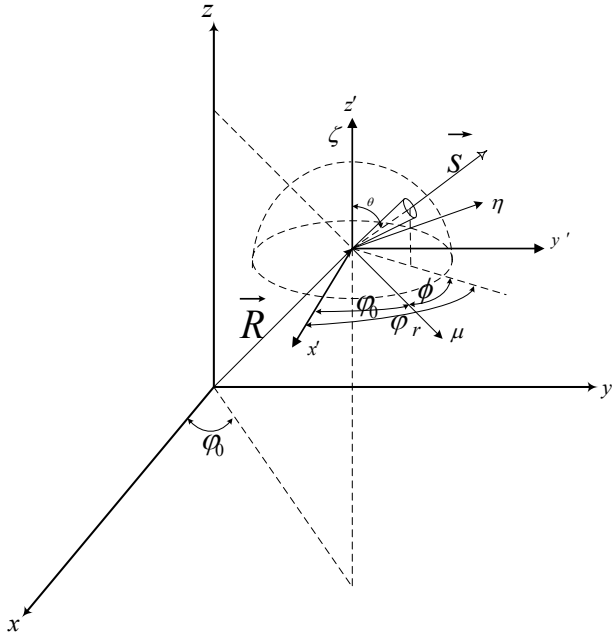In this analysis all boundaries are assumed diffuse-gray where the RTE is subject to the following bound-

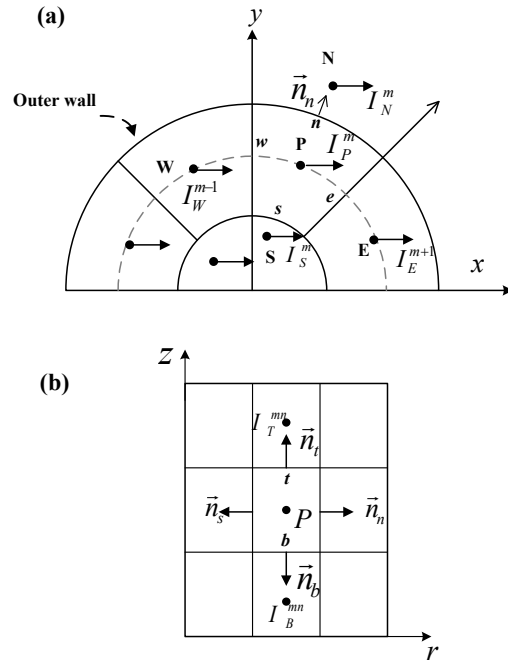*Figure 1. Reference coordinates system for the RTE as given by [6].*

Figure 2. The control volume in a cylindrical enclosure around node P and molecule of nodal points:(a)top view (b)side view.
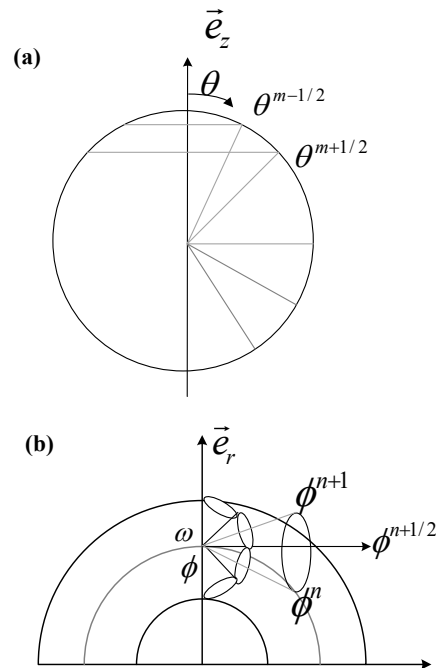

Figure 3. The angular discretization:(a)azimuthal direction (b)polar direction.

ary condition for the intensity on the wall I_w:

$$I_w(R_w, \vec{S}) = \varepsilon_w I_b(R_w)$$
$$+ \frac{1 - \varepsilon_w}{\pi} \int_{\vec{n}_w \cdot \vec{s}' < 0} I(r_w, \vec{s}') d\omega' \quad (4)$$

In a circuit breaker, all boundaries are assumed as black body ($\varepsilon_{wall} = 1$), so for a surface with a specific temperature (T_B) the boundary condition is:

$$I_w(R_w, \vec{S}) = \sigma_B T_B^4 / \pi \quad (5)$$

2.1. Finite Volume Solution for the RTE

The finite volume method (FVM) enforces the conservation laws for discrete volumes (computational mesh) to solve the governing equations in fluid dynamics and heat transfer simulation. Eq. 1 conveys the conservation of radiant energy in a specific direction over a differential control volume and within an infinitesimal control angle.

To solve this equation, the computational domain is discretized as shown in Fig. 2 for a cylindrical domain. The intensity is located on the nodal points P, E, W, S, N, T, and B. Each nodal point P is enclosed by six control surfaces identified by *e, w, s, n, t,* and *b*. Furthermore, direction is divided into discrete solid angles ω^{mn} that are defined for m_{th} polar and n_{th} azimuthal solid angle in a range of $\phi^{n-1/2}$ to $\phi^{n+1/2}$ and $\theta^{m-1/2}$ to $\theta^{m+1/2}$ as shown in Fig. 3. The integration points are located on the surfaces of the control volume [6]. Eq. 3 is integrated over a control volume, V_P, and a control angle ω^{mn} to obtain the discretized form of the RTE:

$$\sum_{i=n,s,t,b,w}^{6} A_i D_i^{mn} I_u i^{mn}$$
$$= [-\kappa_{a,P} I_P^{mn} + \kappa_{a,P} I_{b,P}] \omega^{mn} V_P \quad (6)$$

where A_i is the control surface area and I_b is the black body intensity which is determined with domain temperature and:

$$D_f^l = \int_{\omega^l} \vec{s}.\vec{n_f} d\omega \qquad (7)$$

2.2. Evaluating the Intensity on the Control Surfaces

In a circuit breaker the RTE and the gas dynamics equations are solved on the same grid and due to presence of high gradient in the flow, this grid should be fine enough in order to have accurate results. In the present work, a first order step scheme that is accurate on fine grid is used to evaluate the intensity on the surfaces of the control volume. In each direction, for the surfaces which are located in the upstream of the node P while the intensity on the surface is considered as I_P^{mn} and for the surfaces which are in downstream of the node P the intensity of downstream nodes are:

$$I_{i=n,t,e}^{mn} = I_P^{mn} \qquad (8a)$$

$$I_s^{mn} = I_S^{mn} \qquad (8b)$$

$$I_w^{mn-1/2} = I_W^{mn-1} \qquad (8c)$$

$$I_b^{mn} = I_B^{mn} \qquad (8d)$$

2.3. Final Form of the Equations

Replacing the value of the intensity in Eq. 6, the final form of the equations for the radiant intensity on node P is:

$$a_p^{mn} I_p^{mn} = \sum_{I=N,S,T,B,W} a_I I_I^{mn} + b_P^{mn} \qquad (9)$$

In order to solve this equation explicitly an appropriate marching order is necessary.

2.4. Axisymmetric Extension

The radiant heat transfer is axisymmetric when the intensity does not depend on φ_0 and the intensity is indicated as $I(r, z, \phi, \theta)$. The intensities shown in Fig. 4a are located in the same r, z, and θ. The spatial angular difference $\Delta\varphi_0$ for all points (i=1,2..., 8) is $\pi/4$. The points (i=1,2..., 8) are locate at $\varphi_0 = 7\pi/8, 5\pi/8, 3\pi/8, ...$ respectively, and the angle $\phi_r = 0$. Thus, the angle $\phi = \varphi_r - \varphi_0$ is $-7\pi/8, -5\pi/8, -3\pi/8, ...$ for the intensities $I_1^1, I_2^1, I_3^1, ...$. However, in Fig. 4b the intensities are located at same r, z, and θ and at spatial angle $\varphi_0 = 7\pi/8$, with angular azimuthal angle $\varphi_0 = 0, \pi/4, \pi/2, ...$ for the intensities $I_1^2, I_1^2, I_1^2, ...,$ respectively and the $\phi = 7\pi/8, -5\pi/8, -3\pi/8, ...$ ($\Delta\varphi_0 = \Delta\phi$). Therefore, $r, z, \phi,$ and θ are the same for I_1^m and I_m^1 in Fig. 4a and Fig. 4b. Due to this mapping between intensities in Fig. 4a and Fig. 4b, it is more convenient to solve the domain in Fig. 4a to obtain the intensity for each node.
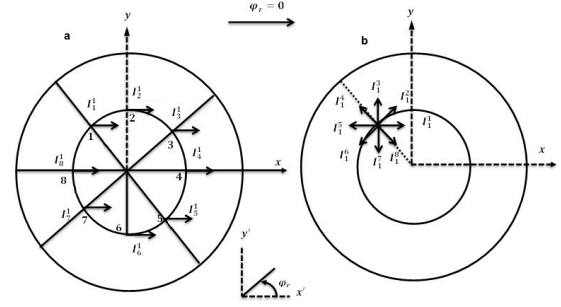

Figure 4. A mapping between the distribution of intensity in cylindrical coordinate system and intensity at specific point in all directions.

2.5. Solution Procedure

A marching order map for nodes is employed to solve the radiant heat transfer within a non-scattering cylindrical medium. For $\theta < \pi/2$, the marching order is from outer wall to the center point for segment 1 in Fig. 2a for each z level from bottom to the top of the cylinder Fig. 2b. For the segments with $\phi_0 > \pi/2$, the marching is from center point to the wall for each z level from bottom of the cylinder to the top of it. The same manner is carried out for all the segments with $\theta > \pi/2$, but the marching order in z direction is from the top to the bottom. The nodal intensity is obtained explicitly for a given medium temperature if the enclosure walls are black.

3. Results and Discussions

3.1. Isothermal cylinder

Figure 5 shows the results of a verification study for a cylindrical geometry filled with isothermal gas at T=1000 K. The cylinder has a $r = 1$ m radius and its length is 2 m. The temperature at the cylindrical wall and at both ends of the cylinder is fixed at $T = 0$ K. The results show the normalised radiative flux on the cylindrical wall for three different values of the optical thickness (defined as $\tau = r\kappa_a$). Two cartesian grids are computed with, respectively, 17×33 and 50×75 grid points. For the two cases, the discretization of angular space is 14×16 directions. Results are compared to the analytical solution from ref. [7]. Globally, the results are excellent and accurate, even on coarse grid.

Figure 6 shows the effect of the angular discretization for the same cylindrical case. One can see that an angular discretization using 10×12 directions provides almost the same result as a 14×16 discretisation. Since the computational time increases linearly with the number of directions, the following results will be computed using a 10×10 angular discretization.

3.2. Semi-industrial test case

Figure 7 illustrates the second geometry used to test the present computational approach. The geometry is representative of elements found in circuit-breakers to illustrate the characteristics of the method. As seen
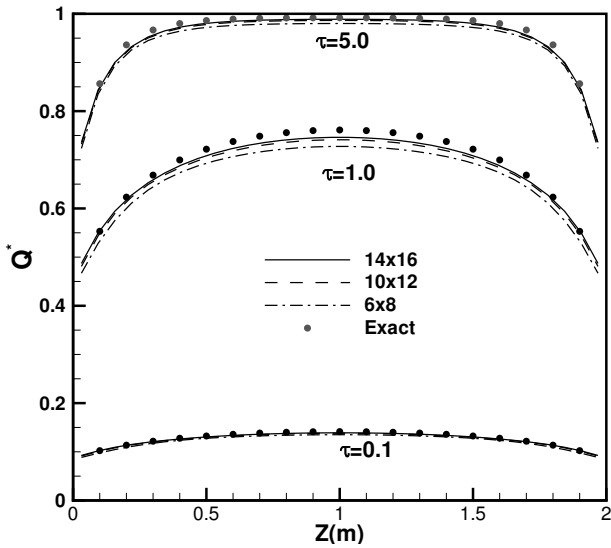
Figure 5. The radiative heat flux on the cylinder wall in various angular grids $N_r \times N_z \times N_\phi \times N_\theta$.
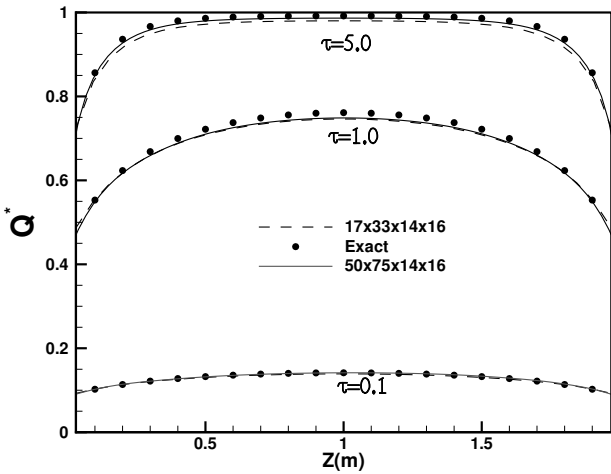

Figure 6. The comparison of the radiative heat flux obtained with numerical simulation on the cylinder wall in various spatial grids $N_r \times N_z \times N_\phi \times N_\theta$.

in Fig. 7, a hot region is placed on the axis with a temperature $T = 1000\,\mathrm{K}$. Two blocking regions are inserted into the domain. The rest of the domain contains a gas at $T = 0\,\mathrm{K}$ with a constant absorption coefficient.

Figures 8, 9 and 10 illustrate a comparison of the normalized radiative heat flux on the upper boundary obtained with various methods. The FVM-MC3 method is described in ref. [5]. It implements an implicit version of the FVM method for the solution of the RTE. The P1-MC3 method is described in ref. [3]. It implements the classical P1 method. Both methods are compared with the present work, for three different values of the absorption coefficient. The FVM-MC3 and the P1-MC3 method are computed on a triangular grid composed of 20780 nodes. The present method use a 20700 nodes Cartesian grid. First, one can observe that the agreement between the two FMV methods is very good. The differences
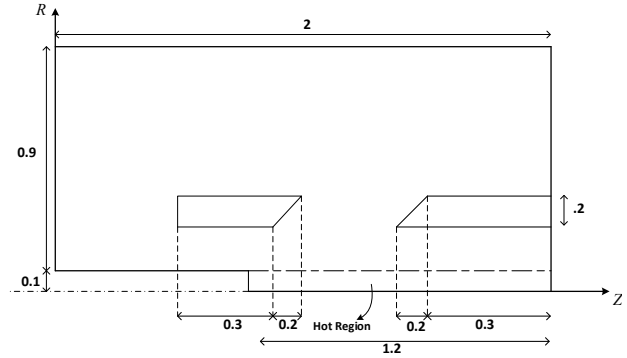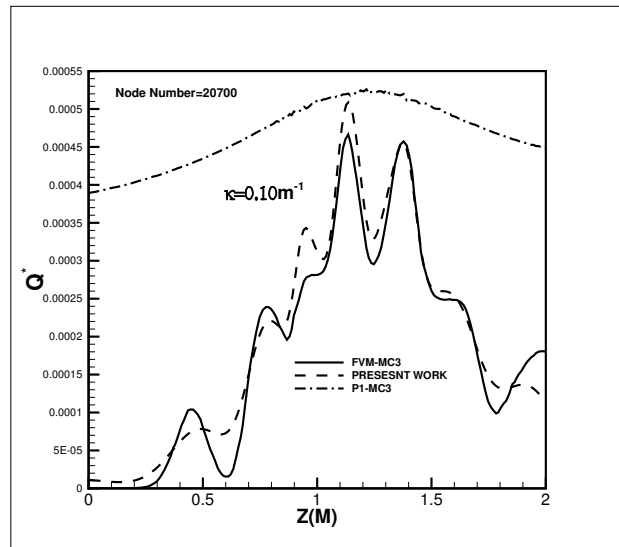

Figure 7. Semi-industrial test case geometry.

Figure 8. The comparison of the radiative heat flux obtained using current numerical approach and results obtained with MC^3 for $\kappa = 0.1\,m^{-1}$.

can be attributed to the different grids used. Second, the results confirm the poor performance of the P1 method for such cases, especially for low and high coefficient of absorption and for long distance propagation of radiation over obstacle in the domain.

3.3. CPU time

The Table 1 give the CPU time required for the radiation computation for the semi-industrial case. It can be observed that on a 10×10 angular discretization, the present method is more that 50 times faster than the previous FVM-MC3. Also, the computation time is close to the one required by the current implementation of the P1 model. This result confirms the very high potential of the method in reducing computation time for the FVM solution of the RTE.

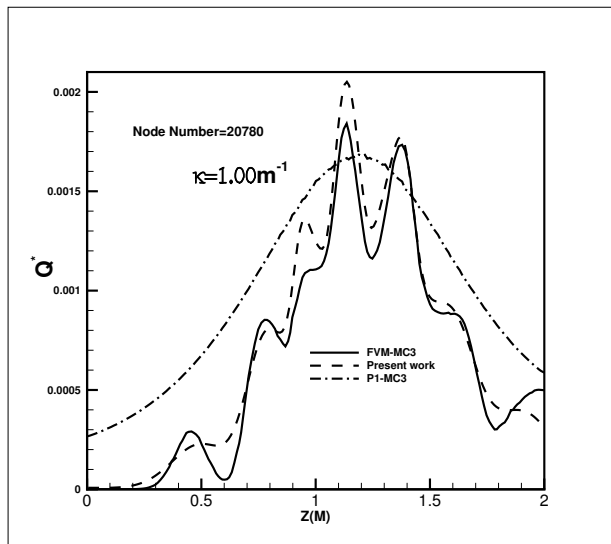| FVM-MC3	P1-MC3	Present Method
40 sec.	0.3 sec.	0.7 sec.

Table 1. Comparison of CPU time

Figure 9. The comparison of the radiative heat flux obtained using current numerical approach and results obtained with MC^3 for $\kappa = 1.0\,m^{-1}$.
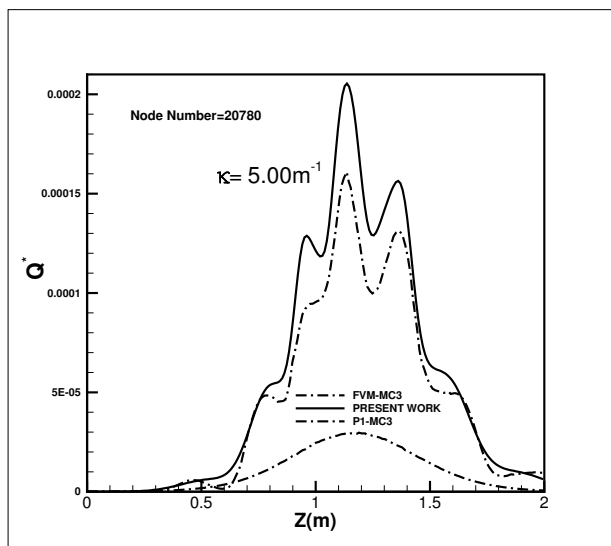

Figure 10. The comparison of the radiative heat flux obtained using current numerical approach and results obtained with MC^3 for $\kappa = 5.0\,m^{-1}$.

4. Conclusion

In the present work, we have described and implemented an explicit version of the FVM for the solution of the RTE in circuit-breakers. The main assumption is that the boundaries of the computational domain can be assumed as black bodies, absorbing all incident radiation. This assumption allows to use a one sweep explicit marching solution procedure of the RTE, reducing the computation time in comparison to implicit methods. The results shows the correctness of the implementation and confirm the CPU saving expected.

References

[1] H. Nordborg and A.A. Iordanidis. Self-consistent radiation based modelling of electric arcs: I. efficient radiation approximations. *Journal of Physics D: Applied Physics*, 41(13):135205, 2008. `doi:10.1088/0022-3727/41/13/135205`.

[2] A.A. Iordanidis and C.M. Franck. Self-consistent radiation-based simulation of electric arcs: II. application to gas circuit breakers. *Journal of Physics D: Applied Physics*, 41(13):135206, 2008. `doi:10.1088/0022-3727/41/13/135206`.

[3] S.D. Eby, J.Y. Trépanier, and X.D. Zhang. Modelling radiative transfer in SF_6 circuit-breaker arcs with the P_1 approximation. *Journal of Physics D: Applied Physics*, 31(13):1578, 1998. `doi:10.1088/0022-3727/31/13/012`.

[4] M.F. Modest. Chapter 16 - the method of spherical harmonics (P_N-approximation). In M.F. Modest, editor, *Radiative Heat Transfer (Third Edition)*, pages 495–540. Academic Press, Boston, 2013.

[5] M. Melot, J.Y. Trépanier, R. Camarero, and E. Petro. Comparison of numerical models in radiative heat transfer with application to circuit-breaker simulations. *Mathematics and Computers in Simulation*, 82(12):2982 – 2996, 2012. `doi:10.1016/j.matcom.2012.07.002`.

[6] M.Y. Kim. Assessment of the axisymmetric radiative heat transfer in a cylindrical enclosure with the finite volume method. *International Journal of Heat and Mass Transfer*, 51(21):5144–5153, 2008. `doi:10.1016/j.ijheatmasstransfer.2008.03.012`.

[7] S. Dua and P. Cheng. Multi-dimensional radiative transfer in non-isothermal cylindrical media with non-isothermal bounding walls. *International Journal of Heat and Mass Transfer*, 18(2):245–259, 1975. `doi:10.1016/0017-9310(75)90157-X`.